Geology

The Miocene elevation of Mount Everest

Aude Gébelin, Andreas Mulch, Christian Teyssier, Micah J. Jessup, Richard D. Law and Maurice Brunel

Geology published online 24 May 2013;
doi: 10.1130/G34331.1

Notes

Geology, published online on 24 May 2013 as doi:10.1130/G34331.1

The Miocene elevation of Mount Everest

Aude Gébelin[1,3], Andreas Mulch[1,2,3], Christian Teyssier[4], Micah J. Jessup[5], Richard D. Law[6], and Maurice Brunel[7]
[1]Biodiversity and Climate Research Centre (BiK-F), Senckenberganlage 25, 60325 Frankfurt, Germany
[2]Institut für Geowissenschaften, Goethe Universität Frankfurt, Altenhöferallee 1, 60438 Frankfurt, Germany
[3]Senckenberg, Senckenberganlage 25, 60325 Frankfurt, Germany
[4]Department of Earth Sciences, University of Minnesota, Minneapolis, Minnesota 55455, USA
[5]Department of Earth and Planetary Sciences, University of Tennessee, Knoxville, Tennessee 37996, USA
[6]Department of Geosciences, Virginia Tech, Blacksburg, Virginia 24061, USA
[7]Géosciences Montpellier UMR 5243, Université Montpellier 2, 34095 Montpellier, France

ABSTRACT

The Neogene elevation history of the Mount Everest region is key for understanding the tectonic history of the world's highest mountain range, the evolution of the Tibetan Plateau, and climate patterns in East and Central Asia. In the absence of fossil surface deposits such as paleosols, volcanic ashes, or lake sediments, we conducted stable isotope paleoaltimetry based on the hydrogen isotope ratios (δD) of hydrous minerals that were deformed in the South Tibetan detachment shear zone during the late Early Miocene. These minerals exchanged isotopically at high temperature with meteoric water (δD_{water} = −156‰ ± 5‰) that originated as high-elevation precipitation and infiltrated the crustal hydrologic system at the time of detachment activity. When compared to age-equivalent near-sea-level foreland oxygen isotope ($\delta^{18}O$) paleosol records ($\delta^{18}O_{water}$ = −5.8‰ ± 1.0‰), the difference in $\delta^{18}O_{water}$ is consistent with mean elevations of ≥5000 m for the Mount Everest area. Mean elevations similar to modern suggest that an early Himalayan rain shadow may have influenced the late Early Miocene climatic and rainfall history to the north of the Himalayan chain.

INTRODUCTION

How the elevation of the Himalayan mountain range, including the Mount Everest region, has evolved over Neogene time is of particular interest for understanding collisional tectonics, orogenic plateau and summer monsoon development (e.g., Harrison et al., 1992; Boos and Kuang, 2010), global climate change, and evolutionary and biotic changes in Central Asia (e.g., Liu et al., 2006). Quantifying the evolution of topography provides a link among Earth surface changes, atmospheric processes, and orogen-scale tectonics. Although paleoelevation reconstruction is challenging (Mulch and Chamberlain, 2007), stable isotope paleoaltimetry has emerged as a reliable method to gauge the evolution of topography in eroded orogens (e.g., Garzione et al., 2000; Poage and Chamberlain, 2001; Mulch et al., 2004; Rowley and Currie, 2006; Gébelin et al., 2012). Stable isotope paleoaltimetry relies on the systematic relationship between depletion in deuterium (D) and ^{18}O of meteoric water and the elevation of an orographic barrier over which air masses rise and cool; as a result, oxygen ($\delta^{18}O$) and hydrogen (δD) isotope ratios of rainfall scale with elevation on the windward side of a mountain range (e.g., Poage and Chamberlain, 2001; Rowley et al., 2001). In contrast, an orographic rain shadow commonly develops on the leeward side and promotes arid to semiarid conditions, where low $\delta^{18}O$ and low δD precipitation, as well as above-ground and subsurface evaporation (e.g., Quade et al., 2011), result in $\delta^{18}O$ and δD values of rainfall that no longer correlate directly with elevation. Here we reconstruct the Early Miocene paleoelevation of the Mount Everest region to better understand the impact of high topography on Himalayan erosional and deformational processes and to evaluate the time at which the Himalayan belt was sufficiently high to promote a leeward rain shadow.

None of the commonly used geologic materials (paleosols, volcanic ashes, or lacustrine sediments) amenable to record the stable isotopic composition of Early Miocene meteoric water are preserved within the highly erosive Himalayan range. In the following we use an approach that was pioneered in the North American Cordillera (Mulch et al., 2004) and is based on water-rock interaction in crustal-scale shear zones that we reference to near-sea-level foreland rainfall records (e.g., Gébelin et al., 2012; Campani et al., 2012). We determine δD values of meteoric water that permeated the South Tibetan detachment (STD) system in the Mount Everest region and exchanged isotopically with hydrous silicates (mica, amphibole) during deformation. If mineral-water hydrogen isotope equilibrium was achieved during deformation and recrystallization, δD values measured in synkinematic minerals likely reflect 10^5–10^6 yr of isotopic exchange, and can be retrieved through experimentally calibrated isotope exchange parameters (e.g., Mulch et al., 2004; Gébelin et al., 2011). For our paleoaltimetry reconstruction, we compare δD values from the high-elevation STD to age-equivalent $\delta^{18}O$ values within pedogenic carbonate from near-sea-level Siwalik foreland basin paleosols that record Miocene rainfall conditions in the Himalayan foothills. The difference in $\delta^{18}O_{water}$ obtained by these two approaches is consistent with late Early Miocene mean elevations of ≥5000 m for the Mount Everest region.

GEOLOGICAL SETTING AND RESULTS

We collected oriented samples from the STD in the underlying mylonitic footwall in the Rongbuk Valley, north of Mount Everest (Fig. 1; Figs. DR1–DR3 in the GSA Data Repository[1]). In this area, the STD consists of the upper (brittle) Qomolangma detachment

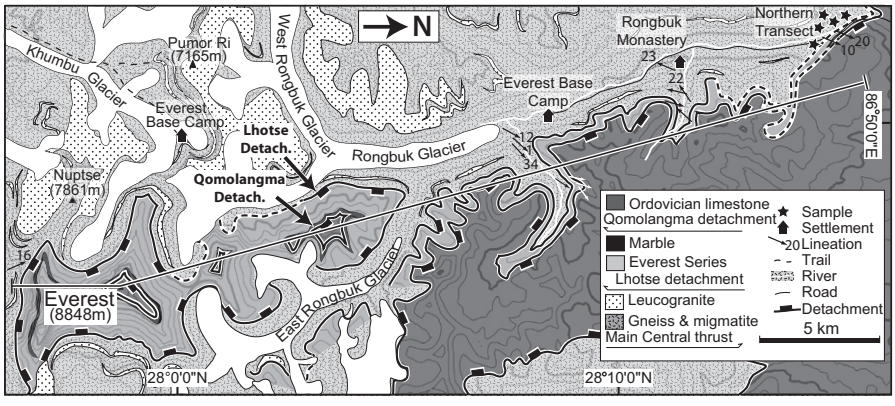

Figure 1. Simplified geological map of Mount Everest region and Rongbuk Valley (after Searle, 2003; Jessup et al., 2006, 2008).

[1]GSA Data Repository item 2013220, Figure DR1 (north-south cross section across Mount Everest), Figure DR2 (sampling sites), Figure DR3 (DEM from which modern mean elevations have been calculated), and Table DR1 (hydrogen isotope results and methods), is available online at www.geosociety.org/pubs/ft2013.htm, or on request from editing@geosociety.org or Documents Secretary, GSA, P.O. Box 9140, Boulder, CO 80301, USA.

and the lower (ductile) Lhotse detachment shear zone that merge northward (Carosi et al., 1998) and collectively separate upper plate, nonmetamorphosed Ordovician limestone from high-grade metamorphic rocks and syntectonic leucogranite below (Carosi et al., 1998; Searle et al., 2003) (Fig. DR1). The shear zone includes marble, calc-silicate, leucogranite, and biotite-sillimanite schist and gneiss. All rocks contain a strong, shallowly northeast dipping foliation (5°–20°N) and NNE-SSW–trending stretching lineations. Kinematic criteria (C-S microstructures, mica fish, and asymmetric porphyroclast tails) indicate top-to-the-north shearing (Burg et al., 1984; Law et al., 2004). Quartz microstructures and c-axis fabrics suggest that rocks in the shear zone deformed at temperatures >500 °C (Law et al., 2004, 2011) (Fig. 2; Table DR1 in the Data Repository). Based on radiometric dating of mylonitic and undeformed leucogranite, the maximum age of ductile shearing is ca. 17 Ma, while brittle faulting on the Qomolangma detachment was likely younger than 16 Ma (Hodges et al., 1998; Murphy and Harrison, 1999; Searle et al., 2003); in the following, we refer to the timing of shearing on this part of the STD as late Early Miocene. Together with quantitative data on strain and vorticity of flow (Jessup et al., 2006), microstructures and quartz c-axis fabrics are interpreted to have developed during top-to-the-north high-temperature shearing associated with southward-directed extrusion of the Himalayan crystalline core (Burg et al., 1984; Law et al., 2004, 2011).

At Rongbuk Valley, we analyzed δD values of biotite and hornblende in 17 samples of sheared leucogranite, pegmatite, biotite schist and/or gneiss, and calc-silicate collected across ~200 m of structural section from the STD into the underlying mylonitic footwall (Fig. 1; Figs. DR1 and DR2; Table DR1). Biotite shows very low δD values of −126‰ to −182‰ within 0–100 m of section, while the base of the section (130–177 m) is characterized by higher biotite δD values (−97‰ to −85‰), typical for δD values in metamorphic rocks (Fig. 2). Similarly, hornblende separates at 24 m and 98 m in the section yield very low δD values of −181‰ and −183‰, respectively. The low δD values within the uppermost 100 m of the section require the presence of low δD meteoric water (Fig. 2) during high-temperature deformation in the STD footwall.

δD values of meteoric water that exchanged with hydrous minerals during STD shearing can be calculated if the hydrogen isotope mineral-water fractionation and the associated exchange temperatures are known (Figs. 2 and 3; Table DR1). Using a deformation and isotopic exchange temperature of ~581 ± 50 °C inferred from the opening angles of quartz c-axes girdles (Law et al., 2011), combined with the calibration of biotite-water hydrogen

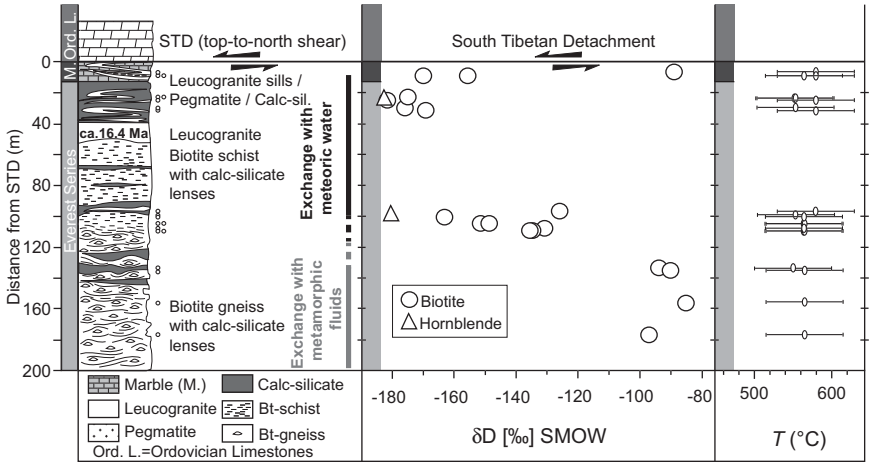

Figure 2. Hydrogen isotope values (δD) of biotite and hornblende from mylonitic rocks in footwall of South Tibetan detachment (STD), lithologic section through STD, and recrystallization temperatures (*T*) based on opening angle of quartz c-axes girdle patterns (Law et al., 2011). Fields for meteoric and metamorphic waters are indicated. SMOW—standard mean ocean water.

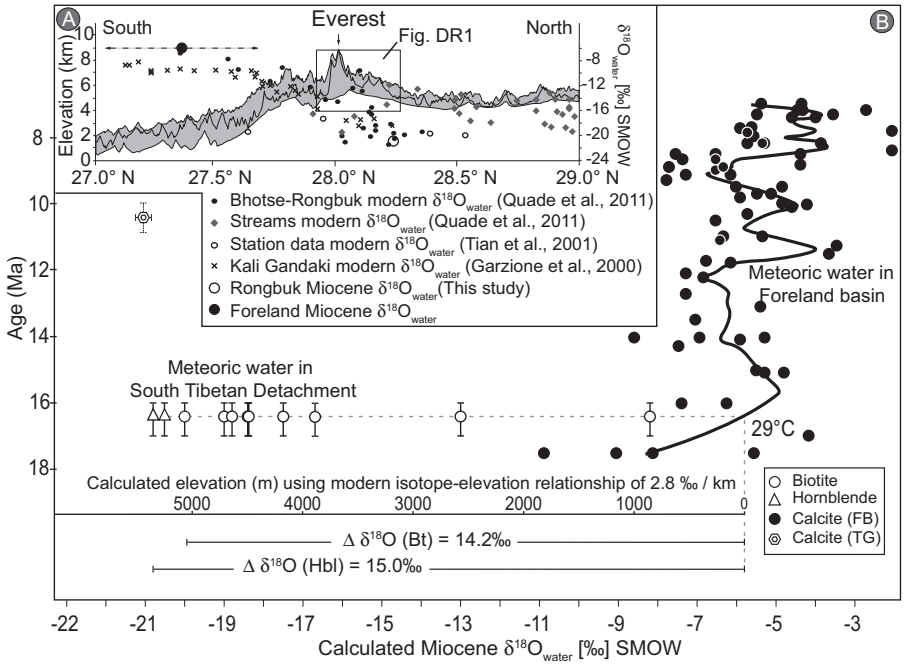

Figure 3. A: Modern $\delta^{18}O_{water}$ (standard mean ocean water, SMOW) values (Quade et al., 2011) along elevation profile (V/H = 6) across Mount Everest (location in Fig. DR3 [see footnote 1]). North-south topographic section (27.00°N, 86.925204°E to 29.00°N, 86.925204°E) is based on unfiltered digital elevation data (90 m accuracy) from Shuttle Radar Topography Mission (SRTM-V4; Farr et al., 2007). Gray area represents elevation of 20-km-wide swath along section with clear δD_{water}-elevation relationship. Modern $\delta^{18}O_{precipitation}$ values in Rongbuk-Tingri and Hermits Gorge areas (~–21‰; Quade et al., 2011) are similar to lowest $\delta^{18}O_{water}$ values calculated from Miocene biotite and hornblende. B: Miocene paleoaltimetry reconstruction of Mount Everest (this study) compared to oxygen isotope record in Siwalik foreland basin (FB; Quade and Cerling, 1995; Quade et al., 1995; Leier et al., 2009). Calculated 7.0–17.5 Ma $\delta^{18}O_{water}$ values for carbonate in foreland are from $\delta^{18}O_{carbonate}$ data (Quade and Cerling, 1995; Quade et al., 1995; Leier et al., 2009), using surface temperature of 29 °C (Quade et al., 2013). White hexagon is calculated $\delta^{18}O_{water}$ from lacustrine carbonate in Thakkhola graben (TG; Garzione et al., 2000). Difference in $\delta^{18}O_{water}$ of ~15‰ between high elevation (South Tibetan detachment) and low elevation (Siwalik foreland basin) is consistent with Miocene paleoelevation of Everest region in excess of 5000 m. Bt—biotite; Hbl—hornblende.

isotope exchange (Suzuoki and Epstein, 1976), $\delta D_{biotite}$ values between 0 m and 100 m of the STD footwall yield δD_{water} values as low as −150‰ +5‰/−4‰. Similarly low δD_{water} values of −156‰ ± 5‰ can be reconstructed from $\delta D_{hornblende}$ = −183‰ in sheared calc-silicate rocks using an exchange temperature of 555 ± 50 °C (Law et al., 2011).

Because single-site paleoaltimetry reconstructions frequently lack adequate knowledge of changes in atmospheric circulation patterns, paleoclimate, and paleoenvironmental conditions, we recast our δD_{water} values as $\delta^{18}O_{water}$ by means of the global meteoric water line ($\delta D = 8 \times \delta^{18}O + 10$; Craig, 1961; Table DR1) and then compare the high-elevation STD record to age-equivalent $\delta^{18}O$ values measured within pedogenic carbonate from Siwalik foreland paleosols. These paleosols record Miocene near-sea-level rainfall conditions in the Himalayan foothills (Quade and Cerling, 1995; Quade et al., 1995; Leier et al., 2009) (Fig. 3B). The relative difference in $\delta^{18}O$ between late Early Miocene meteoric water in the low-elevation Siwalik foreland basin ($\delta^{18}O_{water}$ = −5.8‰ ± 1.0‰ based on $\delta^{18}O$ of pedogenic carbonate and mean annual temperatures of Quade et al., 2013) and the high-elevation precipitation that infiltrated the STD ($\delta^{18}O_{water}$ = −20‰ ± 1‰ to −21‰ ± 1‰ based on δD of biotite and hornblende, respectively) yields $\Delta\delta^{18}O_{water}$ = 14.2‰ ± 1.0‰ (calcite-biotite) and 15.0‰ ± 1.0‰ (calcite-hornblende) (Fig. 3B; Table DR1). Because stable isotopes in precipitation systematically scale with elevation (~2.8‰/km in $\delta^{18}O$ or ~22‰/km in δD; e.g., Poage and Chamberlain, 2001; Quade et al., 2011), this Miocene $\Delta\delta^{18}O_{water}$ between Rongbuk Valley (STD) and the Siwalik basins is consistent with an elevation difference of ~5100 ± 400 m and ~5400 ± 350 m, respectively (error estimate includes isotopic analysis and temperature [Table DR1], but excludes uncertainty in the isotopic lapse rate, which for model elevations of ~5000 m is ±700 m; Rowley, 2007).

DISCUSSION AND IMPLICATIONS

Our paleoelevation estimates (5100–5400 m) indicate that the late Early Miocene central Himalaya was at mean elevations similar to modern (5189 ± 390 m with present-day minimum and maximum values of 4553 m and 5982 m; see Fig. DR3). Furthermore, modern precipitation collected in the Rongbuk-Tingri area, to the northwest of our sampling transect, and the Hermit's Gorge area (Fig. DR1) has $\delta^{18}O_{water}$ values of −21.1‰ to −21.5‰ (Quade et al., 2011; Fig. 3A), almost identical to our calculated Early Miocene δD_{water} (−156‰ ± 5‰) and $\delta^{18}O_{water}$ (−21‰ ± 1‰). Documenting high elevations in the Himalaya since the late Early Miocene puts into perspective a series of observations: (1) the oldest known Siwalik sediments in Nepal (Dumri Formation; Ojha et al., 2009), (2) loess deposition in northern China ca. 22 Ma in a leeward rain shadow environment of the Tibetan-Himalayan orogen (Guo et al., 2002), (3) paleoelevation estimates of 4500 m ± 430 m and 6300 m ± 330 m obtained from carbonates deposited ca. 11 Ma in the Thakkhola graben (Garzione et al., 2000; Fig. 3), (4) low δD values in biotite from leucogranite in the Manaslu region ca. 20 Ma (France-Lanord et al., 1988), and (5) paleoenthalpy and stable isotope results suggesting that the elevation of the southern Tibetan Plateau has remained unchanged for the past 9–15 m.y. (Spicer et al., 2003; Saylor et al., 2009).

A consequence of the high topography of the central Himalaya is enhanced aridity on the Tibetan Plateau over most of the Neogene, resulting in high evaporative water flux over the plateau region. Strongly evaporative conditions may have shifted lake and near-surface groundwater $\delta^{18}O$ to higher values, which could lead to an underestimation of Miocene Tibetan Plateau elevation when assessed through the stable isotopic record of surface deposits. In addition, a strong Himalayan orographic rain shadow causes isotopically D (and ^{18}O) depleted precipitation over the plateau region, such that any freshwater stable isotope–based paleoelevation reconstruction from the plateau interior may be biased by rainout that occurred upstream along the Himalayan flanks. Collectively, stable isotope records on the Tibetan Plateau register the combined effects of local evaporation and Himalayan rainout, resulting in paleo–meteoric water compositions that do not necessarily correlate with plateau elevation.

The low biotite and hornblende δD values within the STD indicate that meteoric fluids penetrated the ductile segment of the extensional system during mylonitic deformation. Two conditions favor the downward flow of surface fluids to the brittle-ductile transition zone (Person et al., 2007): (1) upper crustal extension enhances porosity and permeability and permits fracture-dominated flow of meteoric fluids down to the brittle-ductile transition; and (2) sustained high heat flow induces buoyancy-driven fluid convection. The latter condition was likely met when synmylonitization leucogranite bodies intruded the STD footwall. In addition, the hydraulic head generated in high-relief areas may be an important driving force for hydrothermal fluid circulation in detachment systems (Person et al., 2007). The interplay among surface topography, orographic rainfall, and heat advection makes the STD system an important orogen-scale structure for fault-controlled hydrothermal activity. It is likely that the presence of meteoric fluids affected the style and rates of normal faulting in the upper plate and ultimately governed the rates of extension-related exhumation of high-grade metamorphic rocks (Fig. 4). Tracking the interaction of deformational processes and surface-derived meteoric fluids in such detachment systems provides a critical link between processes that characterize the internal dynamics of orogens and those that shape the Earth's surface.

ACKNOWLEDGMENTS

This study was funded through the LOEWE (Landes-Offensive zur Entwicklung Wissenschaftlich-ökonomischer Exzellenz) program of the government of the State of Hesse (Germany) Ministry of Higher Education, Research, and the Arts. Teyssier acknowledges support from U.S. National Science Foundation (NSF) grant EAR-0838541, and Law acknowledges support from NSF grant EAR-0207524. We thank S. Dominguez (Montpellier) for support in interpreting Himalayan digital elevation models, and D. Newell and J. Cottle for assistance during field work. Comments and suggestions by J. Quade and an anonymous reviewer are gratefully acknowledged.

REFERENCES CITED

Boos, W.R., and Kuang, Z., 2010, Dominant control of the South Asian monsoon by orographic

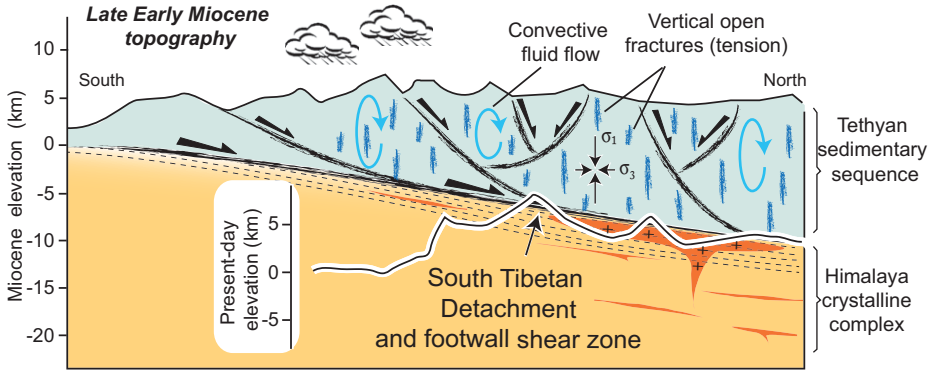

Figure 4. Sketch illustrating hydrothermal system of active South Tibetan detachment (STD) during late Early Miocene. Precipitation sourced at high elevation penetrates down to brittle-ductile transition through synextensional brittle normal faults within Tethyan Himalayan Sequence. Neocrystallized synkinematic hydrous silicates equilibrate with evolved meteoric water in STD where convection of fluids is enhanced by heat advection and hydraulic head created by high-amplitude topography. Schematic present-day Everest elevation profile is given for reference within Miocene section.

insulation versus plateau heating: Nature, v. 463, p. 218–222, doi:10.1038/nature08707.

Burg, J.P., Brunel, M., Gapais, D., Chen, G.M., and Liu, G.H., 1984, Deformation of leucogranites of the crystalline Main Central Sheet in southern Tibet (China): Journal of Structural Geology, v. 6, p. 535–542, doi:10.1016/0191-8141(84)90063-4.

Campani, M., Mulch, A., Kempf, O., Schlunegger, F., and Mancktelow, N., 2012, Miocene paleotopography of the Central Alps: Earth and Planetary Science Letters, v. 337–338, p. 174–185, doi:10.1016/j.epsl.2012.05.017.

Carosi, R., Lombardo, B., Molli, G., Musumeci, G., and Pertusati, P.C., 1998, The South Tibetan detachment system in the Rongbuk valley, Everest region. Deformation features and geological implications: Journal of Asian Earth Sciences, v. 16, p. 299–311, doi:10.1016/S0743-9547(98)00014-2.

Craig, H., 1961, Isotopic variations in meteoric waters: Science, v. 133, p. 1702–1703, doi:10.1126/science.133.3465.1702.

Farr, T.G., and 17 others, 2007, The Shuttle Radar Topography Mission: Reviews of Geophysics, v. 45, p. 1–33, doi:10.1029/2005RG000183.

France-Lanord, C., Sheppard, S.M.F., and Le Fort, P., 1988, Hydrogen and oxygen isotope variations in the High Himalaya peraluminous Manaslu leucogranite: Evidence for heterogeneous sedimentary source: Geochimica et Cosmochimica Acta, v. 52, p. 513–526, doi:10.1016/0016-7037(88)90107-X.

Garzione, C.N., Quade, J., DeCelles, P.G., and English, N.B., 2000, Predicting paleoelevation of Tibet and the Himalaya from $\delta^{18}O$ vs. altitude gradients in meteoric water across the Nepal Himalaya: Earth and Planetary Science Letters, v. 183, p. 215–229, doi:10.1016/S0012-821X(00)00252-1.

Gébelin, A., Mulch, A., Teyssier, C., Heizler, M., Vennemann, T., and Seaton, N.C.A., 2011, Oligo-Miocene extensional tectonics and fluid flow across the Northern Snake Range detachment system, Nevada: Tectonics, v. 30, p. 1–18, doi:10.1029/2010TC002797.

Gébelin, A., Mulch, A., Teyssier, C., Chamberlain, C.P., and Heizler, M., 2012, Coupled basin-detachment systems as paleoaltimetry archives of the western North American Cordillera: Earth and Planetary Science Letters, v. 335–336, p. 36–47, doi:10.1016/j.epsl.2012.04.029.

Guo, Z.T., Ruddiman, W.F., Hao, Q.Z., Wu, H.B., Qiao, Y.S., Zhu, R.X., Peng, S.Z., Wie, J.J., Yuan, B.Y., and Liu, T.S., 2002, Onset of Asian desertification by 22 Myr ago inferred from loess deposits in China: Nature, v. 416, p. 159–163, doi:10.1038/416159a.

Harrison, T.M., Copeland, P., Kidd, W.S.F., and Yin, A., 1992, Raising Tibet: Science, v. 255, p. 1663–1670, doi:10.1126/science.255.5052.1663.

Hodges, K.V., Bowring, S., Davidek, K., Hawkins, D., and Krol, M., 1998, Evidence for rapid displacement on Himalayan normal faults and the importance of tectonic denudation in the evolution of mountain ranges: Geology, v. 26, p. 483–486, doi:10.1130/0091-7613(1998)026<0483:EFRDOH>2.3.CO;2.

Jessup, M.J., Law, R.D., Searle, M.P., and Hubbard, M.S., 2006, Structural evolution and vorticity of flow during extrusion and exhumation of the Greater Himalayan Slab, Mount Everest Massif, Tibet/Nepal: Implications for orogeny-scale flow partitioning, *in* Law, R.D., et al., eds., Channel flow, extrusion, and exhumation in continental collision zones: Geological Society of London Special Publication 268, p. 379–414, doi:10.1144/GSL.SP.2006.268.01.18.

Jessup, M.J., Cottle, J.M., Searle, M.P., Law, R.D., Tracy, R.J., Newell, D.L., and Waters, D.J., 2008, P-T-t-D paths of Everest Series schist: Journal of Metamorphic Geology, v. 26, p. 717–739, doi:10.1111/j.1525-1314.2008.00784.x.

Law, R.D., Searle, M.P., and Simpson, R.L., 2004, Strain, deformation temperatures and vorticity of flow at the top of the Greater Himalayan Slab, Everest Massif, Tibet: Geological Society of London Journal, v. 161, p. 305–320, doi:10.1144/0016-764903-047.

Law, R.D., Jessup, M.J., Searle, M.P., Francsis, M.K., Waters, D.J., and Cotte, J.M., 2011, Telescoping of isotherms beneath the South Tibetan Detachment System, Mount Everest Massif: Journal of Structural Geology, v. 33, p. 1569–1594, doi:10.1016/j.jsg.2011.09.004.

Leier, A., Quade, J., DeCelles, P., and Kapp, P., 2009, Stable isotopic results from paleosol carbonate in South Asia: Paleoenvironmental reconstructions and selective alteration: Earth and Planetary Science Letters, v. 279, p. 242–254, doi:10.1016/j.epsl.2008.12.044.

Liu, J.Q., Wang, Y.J., Wang, A.L., Hideaki, O., and Abott, R.J., 2006, Radiation and diversification within the Ligularia-Cremanthodium-Parasenecio complex (Asteraceae) triggered by uplift of the Qinghai-Tibetan Plateau: Molecular Phylogenetics and Evolution, v. 38, p. 31–49, doi:10.1016/j.ympev.2005.09.010.

Mulch, A., and Chamberlain, C.P., 2007, Stable isotope paleoaltimetry in orogenic belts—The silicate record in surface and crustal geological archives: Reviews in Mineralogy and Geochemistry, v. 66, p. 89–118, doi:10.2138/rmg.2007.66.4.

Mulch, A., Teyssier, C., Cosca, M.A., Vanderhaeghe, O., and Vennemann, T., 2004, Reconstructing paleoelevation in eroded orogens: Geology, v. 32, p. 525–528, doi:10.1130/G20394.1.

Murphy, M.A., and Harrison, T.M., 1999, Relationship between leucogranites and the Qomolangma detachment in the Rongbuk Valley, south Tibet: Geology, v. 27, p. 831–834, doi:10.1130/0091-7613(1999)027<0831:RBLATQ>2.3.CO;2.

Ojha, T.P., Butler, R.F., DeCelles, P.G., and Quade, J., 2009, Magnetic polarity stratigraphy of the Neogene foreland basin deposits of Nepal: Basin Research, v. 21, p. 61–90, doi:10.1111/j.1365-2117.2008.00374.x.

Person, M., Mulch, A., Teyssier, C., and Gao, Y., 2007, Isotope transport and exchange within metamorphic core complexes: American Journal of Science, v. 307, p. 555–589, doi:10.2475/03.2007.01.

Poage, M.A., and Chamberlain, C.P., 2001, Empirical relationships between elevation and the stable isotope composition of precipitation and surface waters: Considerations for studies of paleoelevation change: American Journal of Science, v. 301, p. 1–15, doi:10.2475/ajs.301.1.1.

Quade, J., and Cerling, T.E., 1995, Expansion of C_4 grasses in the Late Miocene of northern Pakistan: Evidence from stable isotopes in paleosols: Palaeogeography, Palaeoclimatology, Palaeoecology, v. 115, p. 91–116, doi:10.1016/0031-0182(94)00108-K.

Quade, J., Cater, J.M.L., Ojha, T.P., Adam, J., and Harrison, T.M., 1995, Late Miocene environmental change in Nepal and the northern Indian subcontinent: Stable isotopic evidence from paleosols: Geological Society of America Bulletin, v. 107, p. 1381–1397, doi:10.1130/0016-7606(1995)107<1381:LMECIN>2.3.CO;2.

Quade, J., Breecker, D.O., Daëron, M., and Eiler, J., 2011, The paleoaltimetry of Tibet: An isotopic perspective: American Journal of Science, v. 311, p. 77–115, doi:10.2475/02.2011.01.

Quade, J., Eiler, J., Daëron, M., and Achyuthan, H., 2013, The clumped isotope geothermometer in soil and paleosol carbonate: Geochimica et Cosmochimica Acta, v. 105, p. 92–107, doi:10.1016/j.gca.2012.11.031.

Rowley, D.B., 2007, Stable isotope-based paleoaltimetry: Theory and validation: Reviews in Mineralogy and Geochemistry, v. 66, p. 23–52, doi:10.2138/rmg.2007.66.2.

Rowley, D.B., and Currie, B.S., 2006, Palaeo-altimetry of the late Eocene to Miocene Lunpola Basin, central Tibet: Nature, v. 439, p. 677–681, doi:10.1038/nature04506.

Rowley, D.B., Pierrehumbert, R.T., and Currie, B.S., 2001, A new approach to stable isotope-based paleoaltimetry: Implications for paleoaltimetry and paleohypsometry of the High Himalaya since the Late Miocene: Earth and Planetary Science Letters, v. 188, 5836, p. 1–17.

Saylor, J.E., Quade, J., Dettman, D., DeCelles, P.G., and Kapp, P.A., 2009, The late Miocene through present paleoelevation history of southwestern Tibet: American Journal of Science, v. 309, p. 1–42, doi:10.2475/01.2009.01.

Searle, M.P., 2003, Geological map of the Everest massif, Nepal and South Tibet: Oxford University Department of Earth Sciences, scale 1:100,000.

Searle, M.P., Simpson, R.L., Law, R.D., Parrish, R.R., and Waters, D.J., 2003, The structural geometry, metamorphic and magmatic evolution of the Everest massif, High Himalaya of Nepal–South Tibet: Geological Society of London Journal, v. 160, p. 345–366, doi:10.1144/0016-764902-126.

Spicer, R.A., Harris, N.B.W., Widdowson, M., Herman, A.B., Guo, S., Valdes, P.J., Wolfe, J.A., and Kelley, S.P., 2003, Constant elevation of southern Tibet over the past 15 million years: Nature, v. 421, p. 622–624, doi:10.1038/nature01356.

Suzuoki, T., and Epstein, S., 1976, Hydrogen isotope fractionation between OH-bearing minerals and water: Geochimica et Cosmochimica Acta, v. 40, p. 1229–1240, doi:10.1016/0016-7037(76)90158-7.

Tian, L., Masson-Delmotte, V., Stievenard, M., Yao, T., and Jouzel, J., 2001, Tibetan Plateau summer monsoon northward extent revealed by measurements of water stable isotopes: Journal of Geophysical Research, v. 106, p. 28,081–28,088, doi:10.1029/2001JD900186.

Manuscript received 19 December 2012
Revised manuscript received 27 February 2013
Manuscript accepted 3 March 2013

Printed in USA